This week: JY Lee PhD Harvard 2020

Advisor Ashvin Vishwanath Collaborator Subir Sachdev

Last week: Shubhayu Chatterjee PhD Harvard 2018

Advisor Subir Sachdev Collaborator Ashvin Vishwanath

Time reversal symmetry

Spin 1/2 $\mathcal{T}: \uparrow, \downarrow \longrightarrow \downarrow, \uparrow$ $\quad \mathcal{T}: e^{-iEt} \rightarrow e^{-iE(-t)} = \left(e^{-iEt}\right)^*$

$\mathcal{K}$

$$\mathcal{T} = e^{-i\frac{\pi}{2}\sigma_y}\mathcal{K} \qquad \mathcal{T}^2 = -1$$

$$\begin{pmatrix} 0 & -1 \\ 1 & 0 \end{pmatrix} \qquad *$$

If $\mathcal{T}H = H\mathcal{T}$ and $H|\psi\rangle = E|\psi\rangle$ then

$$H(\mathcal{T}|\psi\rangle) = \mathcal{T}H|\psi\rangle = E(\mathcal{T}|\psi\rangle)$$

$\mathcal{T}|\psi\rangle$ is a new state degenerate with $|\psi\rangle$ "Kramers Doublet"

Kramers-Intervalley coherent state (K-IVC)

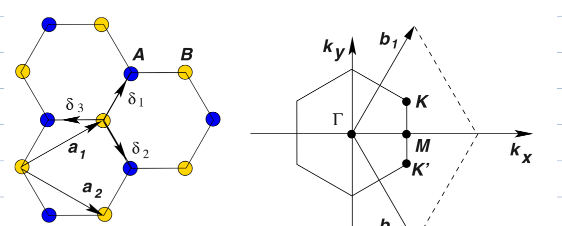

Castro Neto 2009

$C_2: A \longleftrightarrow B \quad K \longleftrightarrow K'$

$\mathcal{T}: K \longleftrightarrow K'$

$(C_2\mathcal{T})^2 = -1$

K-IVC @ charge neutrality

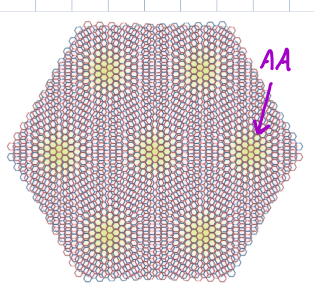

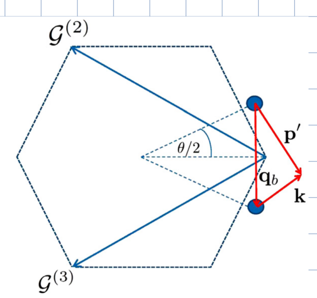

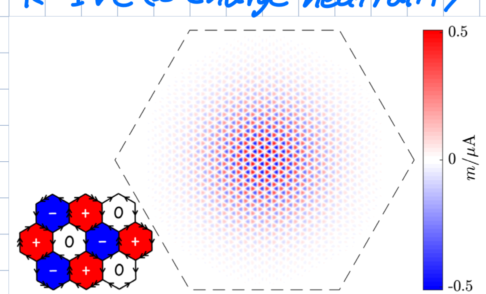

Chatterjee 2020

Spectroscopic Signatures of Correlations (Yonglong Xie, 2019)

Band insulator   Correlated insulators

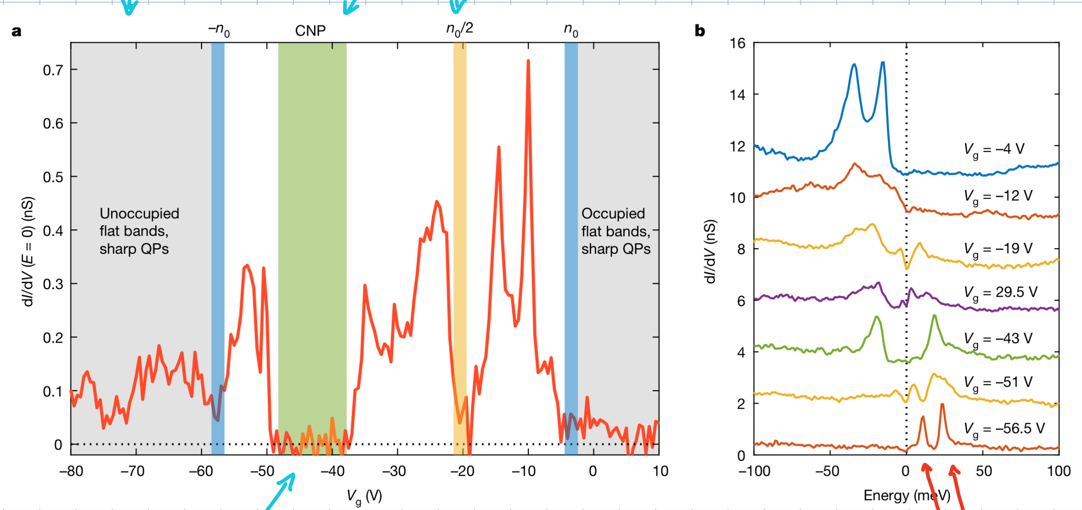

"Charge neutrality"   gating   spectroscopy   Flat bands

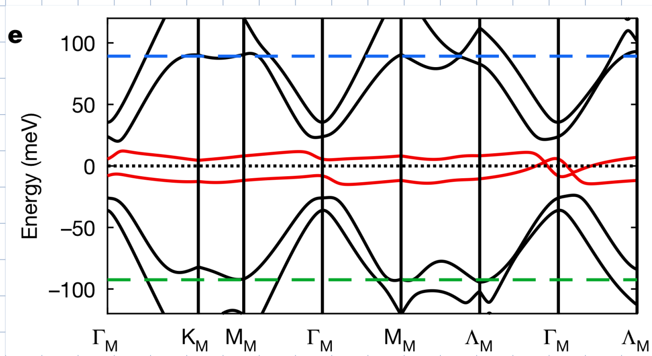

Flat bands

Example correlated insulator (Mott)

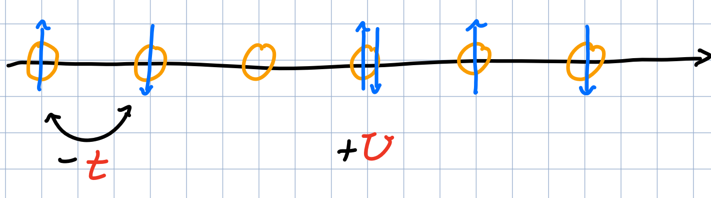

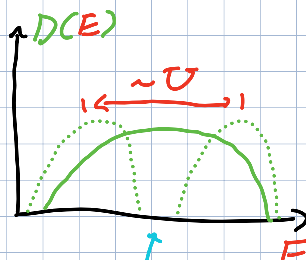

Mott gap

Antiferromagnetism $\sim t^2/U$

Monte Carlo

Hamiltonian H Observable A

Classical thermal average $\langle A \rangle = \sum_c A(c) P(c)$ $\quad P(c) = \frac{1}{Z} e^{-\beta H(c)}$

too many terms $\quad$ don't know Z

$\therefore$ Sample $\{c\}$ with weight $P(c)$: $\langle A \rangle \approx \frac{1}{N} \sum_c{}' A(c)$

Markov chain $c \to c'$ with $P(c')/P(c) = e^{-\beta \Delta E}$

Quantum Monte Carlo

$$\langle A \rangle = \sum_{|\psi\rangle} \langle \psi | A | \psi \rangle P(\psi)$$

e.g. Variational MC seeking ground state

$$E(\alpha) = \frac{\langle \psi_\alpha | H | \psi_\alpha \rangle}{\langle \psi_\alpha | \psi_\alpha \rangle} = \frac{\int d^{3N}\vec{r}\, |\psi_\alpha(\vec{r})|^2 \langle \vec{r} | H | \psi_\alpha \rangle / \psi_\alpha(\vec{r})}{\int d^{3N}\vec{r}\, |\psi_\alpha(\vec{r})|^2}$$

$P_\alpha(\vec{r})$ Sample via MC

$E_\alpha(\vec{r})$ Vary α to minimize E

e.g. path integral (world line) MC (Feynman, 1953)

Example: harmonic oscillator $H = \underbrace{\frac{p^2}{2m}}_{K} + \underbrace{\frac{1}{2} m\omega^2 x^2}_{V}$ $\quad [x,p] = i\hbar$ $\quad [K,V] \neq 0$

$Z = \mathrm{Tr}\, e^{-\beta H}$ $\quad \beta = \frac{1}{k_B T} \longleftrightarrow i\frac{t}{\hbar}$

Subdivide time into slices: $\beta = L\Delta\tau$ $\quad e^{-\Delta\tau H} = e^{-\Delta\tau K} e^{-\Delta\tau V} + O(\Delta\tau^2)$

$$Z = \mathrm{Tr}\,(e^{-\Delta\tau K} e^{-\Delta\tau V})^L = \sum_{x_1 x_2 \cdots x_L} \langle x_1 | e^{-\Delta\tau K} e^{-\Delta\tau V} | x_2 \rangle \langle x_2 | e^{-} \cdots \langle x_L | e^{-\Delta\tau K} e^{-\Delta\tau V} | x_1 \rangle$$

$$\langle x_1 | e^{-\Delta\tau K} e^{-\Delta\tau V} | x_2 \rangle = \langle x_1 | e^{-\Delta\tau K} | x_2 \rangle e^{-\Delta\tau V(x_1)} = e^{-\frac{1}{2} m \left(\frac{x_1 - x_2}{\Delta\tau}\right)^2 \Delta\tau} e^{-\Delta\tau V(x_1)}$$

$\sum_p |p\rangle\langle p|$

$$Z = \int d^L\vec{x}\, e^{-\Delta\tau S_{cl}} \qquad S_{cl} = \sum_{l=1}^{L} \left\{ \frac{1}{2} m \left(\frac{x_l - x_{l+1}}{\Delta\tau} \right)^2 + V(x_l) \right\}$$

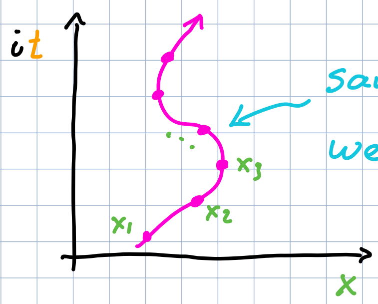

Sample wiggling curves via classical MC

weights $P(\vec{x})$ $\qquad \langle A \rangle = \sum'_{\vec{x}} A(\vec{x})$

Fermion sign problem

$P(\vec{x}) < 0$ for some multifermion $\vec{x}$

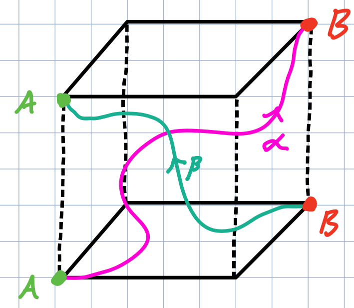

Possible solution (?):

$$\langle A \rangle = \frac{\sum_{\vec{x}} P(\vec{x}) A(\vec{x})}{\sum_{\vec{x}} P(\vec{x})} = \frac{\sum \mathrm{sgn}(x) |P(x)| A(x) / \sum |P(x)|}{\sum \mathrm{sgn}(x) |P(x)| / \sum |P(x)|}$$

$$= \frac{\langle A \rangle_{|P|}}{\langle \mathrm{sgn} \rangle_{|P|}}$$

often $\langle \mathrm{sgn} \rangle \to 0$

Trick: $\mathrm{Tr} \prod_l e^{-\Delta\tau h(l)} = \det\left(1 + \prod_l e^{-\Delta\tau h(l)}\right)$

If $\exists\, \mathcal{T}'$ s.t. $[H, \mathcal{T}'] = 0$ $\quad \mathcal{T}'^2 = -1$ then eigenvalues come in pairs $\Rightarrow \det > 0$

$\mathcal{T}' = C_2 \mathcal{T}$

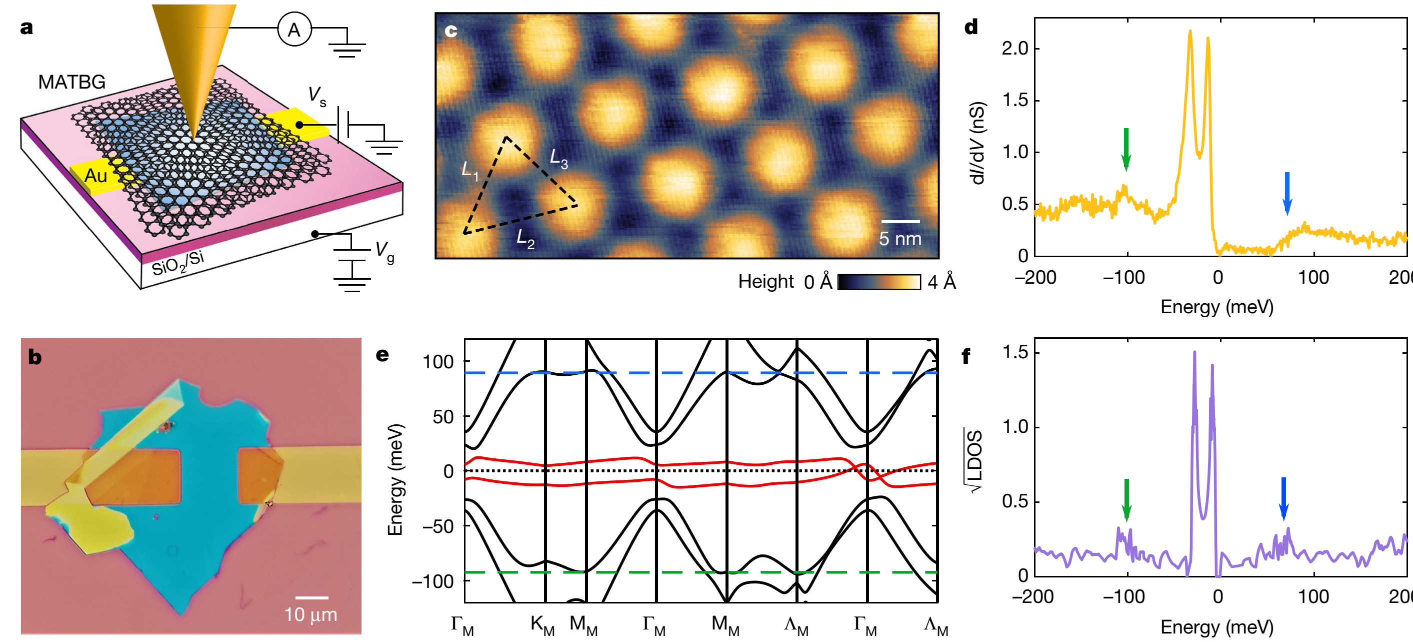

Fig. 1 | Non-interacting spectroscopic properties of MATBG. **a**, Schematic of the STM setup on MATBG devices. **b**, Optical image of the device. **c**, STM topography showing the moiré superlattice with a twist angle θ of 1.01°. **d**, Scanning tunnelling spectrum measured on an AA site for slight electron doping ($V_g = -4$ V, bias voltage $V_{set} = 200$ mV, current $I_{set} = 120$ pA, modulation voltage $V_{mod} = 1$ mV). The blue and green arrows mark the step-like features at higher and lower energies, respectively. **e**, Band structure calculated using the continuum model including the effects of strain and relaxation. $\Gamma_M\Lambda_M$ is a non-high-symmetry direction along which the Dirac points (locally protected by $C_{2z}T$ symmetry) are located. The black dotted line indicates the Fermi level. The blue (green) dashed line corresponds to the van Hove singularities of the first conduction (valence) remote band. **f**, Corresponding $\sqrt{\mathrm{LDOS}}$ (offset by -17 meV) calculated on an AA site. The blue and green arrows mark the van Hove singularities of the first conduction and valence remote bands, respectively.

remote to the flat bands. We have repeated similar local modelling of the dI/dV spectra measured at AA sites using information extracted from topographies at other locations of our devices (see Extended Data Fig. 1). The description of the local spectra is satisfactory when disorder is weak, and when the double peaks associated with the flat bands are either below or above the chemical potential.

The breakdown of this single-particle description of the spectroscopic properties of MATBG when interactions are important becomes evident when we study the evolution of the quasiparticle spectra in our device as a function of electron density controlled by V_g. Figure 2 shows dI/dV measurements on the AA region as a function of V_g, which spans three different regions of occupation for the two flat bands: when the flat bands are both occupied ($V_g > -5.5$ V), when they are being depleted ($-53.5\text{ V} < V_g < -5.5$ V), and after they have been depleted ($V_g < -53.5$ V). The rate of the shift of the flat-band peaks with V_g reflects the DOS at the Fermi level. Therefore, a change in slope of the lines in Fig. 2a signals a transition in band filling. The nearly vertical features signal the slow change of occupation of the flat bands with large DOS. In the range $-58\text{ V} < V_g < -53.5$ V, the change in slope might be related to the presence of an energy gap between the flat bands and the remote bands (estimated to be around 15 meV, which is roughly consistent with the calculated band structure in Fig. 1e). When the nearly flat bands are filled or fully depleted, the spectra—which are individually plotted in Fig. 2b, e—show relatively sharp double peaks at all gate voltages, and the widths of these peaks change weakly with their energy separation to the Fermi level (see Extended Data Fig. 2 and Methods). As described above, these spectra are consistent with those calculated from a non-interacting model that includes the effects of strain and relaxation. However, the most notable change in the quasiparticle spectra occurs when one of the flat bands begins to overlap with the Fermi level, as demonstrated by contrasting the data in Fig. 2c, d with those in Fig. 2b, e. In this region, as one of the flat bands is being depleted, not only does the peak associated with that band near the Fermi level develop substantial features and broaden, but the peak associated with the other valence (conduction) band below (above) the Fermi level is also substantially modified. Notably, the strong distortion of the shape of the quasiparticle spectra—which is caused by interactions during the partial filling of the flat bands—spans an energy range (30–50 meV) that is wider than both the separation of the flat bands to the remote bands and the apparent bandwidths of the flat bands, as measured when fully occupied or unoccupied. This observation demonstrates that the largest energy scale for determining the properties of MATBG at partial filling of the flat bands is set by electron–electron interactions. This signature of strong correlations occurs not just at commensurate fillings, but over all doping ranges for which transport studies[1,2,11,12] have found superconductivity in this system below 1 K.

To further relate our spectroscopic measurements to the transport properties of MATBG, in Fig. 3 we plot the tunnelling conductance at zero energy dI/dV(0)—which is a measure of the DOS at the Fermi level—as a function of V_g. From the changes in dI/dV(0) and the measured energies of the van Hove singularity peaks in Fig. 2, we identify the V_g values that correspond to the point at which there is full local depletion of the conduction or valence flat bands ($n = \pm n_0$, where n and n_0 denote the carrier density of the system and that of a moiré band, respectively); at this point, the transport measurements reveal evidence for a band insulator. Further assignment of the occupation level within the flat bands with V_g is made complicated in our experiments by the presence of the STM tip (see Methods and Extended Data Fig. 3). Focusing on the gate region of V_g at which we are depleting the conduction flat band, a region where the tip-induced effects are minimal, we find some features in the tunnelling spectra that correlate with the transport studies. Most notably we find that, at half-filling of the conduction band ($n = n_0/2$)—where transport measurements reveal the strongest insulating behaviour—dI/dV(0) vanishes and a gap-like feature appears in the spectrum. Recent STM studies of MATBG have reported a similar gap feature, but the suppression of the DOS at the Fermi level was less than 50%[9,10]. However, we caution that this gap at half-filling is much larger (about 20 times) than that observed in transport measurements, and may be related to a soft gap observed at other doping levels (Fig. 2c). Interactions, together with the localization of electrons either by disorder or large magnetic fields, are well known to induce soft Coulomb gaps in tunnelling spectroscopy[26–28]. Close to the